IN VITRO 3D PHENOTYPIC DRUG SCREEN IDENTIFIES CELASTROL AS AN EFFECTIVE IN VIVO INHIBITOR OF POLYCYSTIC KIDNEY DISEASE

Tijmen H. Booij[1,2,#], Wouter N. Leonhard[3,#], Hester Bange[4], Kuan Yan[4], Michiel Fokkelman[1], Anna J. Plugge[3], Kimberley A.M. Veraar[3], Johannes G. Dauwerse[3], Gerard J.P. van Westen[5], Bob van de Water[1], Leo S. Price[1,4,¥], Dorien J.M. Peters[3,¥,*].

[1]Division of Toxicology, Leiden Academic Centre for Drug Research (LACDR), Leiden University, Leiden, The Netherlands

[2]NEXUS Personalized Health Technologies, ETH Zürich, Switzerland

[3]Department of Human Genetics, Leiden University Medical Center (LUMC), Leiden, The Netherlands

[4]OcellO B.V., Leiden, The Netherlands

[5]Division of Medicinal Chemistry, Leiden Academic Centre for Drug Research (LACDR), Leiden, The Netherlands

[#] Authors contributed equally

[¥] Authors contributed equally

* Correspondence to: Dorien J.M. Peters, E-mail: d.j.m.peters@lumc.nl

Short Title

Celastrol to treat PKD

Keywords

PKD, celastrol, pyrvinium pamoate, high-content screening, 3D

Abstract

Polycystic kidney disease (PKD) is a prevalent genetic disorder, characterized by the formation of kidney cysts that progressively lead to kidney failure. The currently available drug tolvaptan is not well tolerated by all patients and there remains a strong need for alternative treatments. The signaling rewiring in PKD that drives cyst formation is highly complex and not fully understood. As a consequence, the effects of drugs are sometimes difficult to predict. We previously established a high throughput microscopy phenotypic screening method for quantitative assessment of renal cyst growth. Here, we applied this 3D cyst growth phenotypic assay and screened 2320 small drug-like molecules, including approved drugs. We identified 81 active molecules that inhibit cyst growth. Multi-parametric phenotypic profiling of the effects on 3D cultured cysts discriminated molecules that showed preferred pharmacological effects above genuine toxicological properties. Celastrol, a triterpenoid from *Tripterygium Wilfordii*, was identified as a potent inhibitor of cyst growth *in vitro*. In an *in vivo* iKspCre-*Pkd1*^{lox,lox} mouse model for PKD, celastrol inhibited the growth of renal cysts and maintained kidney function.

Introduction

Autosomal Dominant Polycystic kidney disease (ADPKD) affects approximately 1 in 2500 people (Willey, et al., 2017). Patients will develop renal failure as a result of progressive growth of renal cysts, which interfere with normal kidney function. The disease is caused by mutations in the *PKD1* or *PKD2* gene, encoding polycystin-1 or polycystin-2, respectively (Torres, et al., 2007). These proteins are expressed in several cellular compartments and form multimeric protein complexes, that modulate multiple signaling pathways, which in concert control essential cellular functions such as proliferation, apoptosis, cell adhesion and differentiation (Torres and Harris, 2014). However, how mutations in the PKD genes cause the development of renal cysts is still not fully understood. In addition, we know little about how the signaling pathways involved in driving renal cyst growth are interconnected, and how they contribute to this process. As a consequence, it is also poorly understood how certain compounds that are under investigation for their therapeutic potential, exert their 'cyst-reducing' properties and why certain therapies become less effective at the more progressive stages.

Currently only one drug, tolvaptan (Jinarc), is marketed for the treatment of PKD. This drug has massive diuresis as a side-effect, which may limit compliance of otherwise asymptomatic

patients (Torres, et al., 2012). Because PKD patients require therapy for many decades, it is critical to improve the balance between side-effects and preventing cyst growth. A possibility to achieve this goal is by combination therapy with multiple effective drugs, allowing for dose reduction, or the identification of more effective drugs with fewer side effects.

To identify new drug candidates that prevent cyst growth, we previously developed a 3D cyst culture-based high-throughput screening platform, which can be used to screen large libraries of molecules for the identification of cyst-inhibiting compounds (Booij, et al., 2017). This 3D assay uses phenotypic profiling of cysts as a measure of compound efficacy. Phenotypic screening can enable the identification of effective molecules irrespective of their mechanism of action and without a comprehensive understanding of the pathophysiology and can be effective at identifying first-in-class treatments (Swinney, 2013).

Here, we applied this screening platform to screen 2320 drug-like molecules to identify effective inhibitors of cyst-growth. Using phenotypic profiling, molecules were pre-selected for *in vivo* testing based on desirable activity and safety. In two independent experiments, we report the potent activity of celastrol, a triterpenoid from *Tripterygium Wilfordii*, at inhibiting cyst growth and maintaining kidney function in an iKspCre-*Pkd1*^{lox,lox} mouse model.

Results

Screening a small-molecule library to identify inhibitors of cyst growth

To identify new molecules that can potentially be used for the treatment of PKD, we screened a SPECTRUM compound library, consisting of 2320 molecules, including kinase inhibitors, natural molecules and FDA-approved drugs. We cultured epithelial cysts from mIMCD3 cells with short hairpin-mediated reduced *Pkd1* expression (mIMCD3 sh*Pkd1*) in 384-well plates in protein hydrogels. Forskolin is known to enhance cyst swelling *in vitro* (Mangoo-Karim, et al., 1989) and is known to activate adenylyl cyclase to induce cyclic adenosine monophosphate (cAMP) production, a central mediator of cystogenesis (Devuyst and Torres, 2013). Following exposure to forskolin, we co-exposed the cysts to control compounds or test compounds of the SPECTRUM library at 1 μM (Supplementary Figure S1). After imaging and calculating cyst size using phenotypic measurements, we ranked the molecules on their potency to inhibit cyst growth as presented in Figure 1A, top panel. As criterion for hit selection, molecules were selected that were at least one standard deviation below the stimulated control condition (2.5 μM forskolin).

As a result, 81 cyst-inhibiting hits were identified (Figure 1A, bottom panel). All hits were re-screened at six concentrations in triplicate wells using RNA-guided *FokI* nuclease-mediated (Tsai, et al., 2014) *Pkd1*-knockout cells (mIMCD3 *Pkd1*$^{-/-}$; Supplementary Figure S2A and B), confirming the activity of 66.6% of the molecules (54 molecules with cyst growth inhibition >50% at 1 μM).

To get more insight into the molecules that were active in our screen, we listed the molecules according to their bioactivities described in the manufacturer's datasheet. It is important to note that some molecules do not belong exclusively to one class and may have dual bioactivities. An evaluation of the 81 hits revealed that the largest group of selected hits were molecules known to have an antineoplastic mechanism of action (25.9% of our hits compared to 4.9% of the library; Figure 1B and C).

Since most ADPKD patients will need drug treatment for decades, antineoplastic drugs are unlikely to become therapeutic candidates. Therefore, we applied linear discriminant analysis (LDA) on measured phenotypic parameters (with correlation <0.85), to discriminate known toxic molecules from stimulated- and unstimulated controls. This strategy allowed us to separate most antineoplastic molecules from molecules with a different mode of action (Supplementary Figure S3A and B). For all molecules, we determined the proximity in feature space to the unstimulated control group as a measure of desirable efficacy. Supplementary Figure S3C presents this distance as a color scale from yellow to blue. While most anti-infective and antihelmintic retained their favorable activity (distance <50 at 1 μM), most antineoplastic molecules remained distant from the favorable (and small) control cysts phenotype.

Celastrol inhibits cyst growth dose-dependently

Based on these results, we found that celastrol (Figure 2A), a triterpenoid extracted from *Tripterygium Wilfordii* (Wong, et al., 2012), and pyrvinium pamoate, an antihelmintic drug (Jung, 1976) and WNT inhibitor (Thorne, et al., 2010) (Supplementary Figure S4A), were very potent at inhibiting cyst growth *in vitro*. Celastrol appeared to induce phenotypes associated with toxicity only at high concentrations (≥316 nM), and potently inhibited forskolin-induced cyst growth at 100 nM (Figure 2B and C), with effects becoming apparent after 48-h co-treatment with forskolin (Supplementary Figure S5A). We also report that at concentrations up to 10 μM, celastrol shows high inhibitory activity whereas tolvaptan failed to show activity at this

concentration (Supplementary Figure S5B), likely because of low expression of the Vasopressin V2 receptor in this particular cell line (unpublished). Interestingly, several closely-related structural analogues of celastrol, dihydrocelastrol and dihydrocelastryl diacetate, displayed a similar activity profile (Supplementary Figure S5C and D). Pyrvinium pamoate showed no indication of toxicity even at high concentrations (Supplementary Figure S4B).

To determine if the inhibition shown by celastrol was dependent on cAMP induction by forskolin, we assessed whether it could inhibit cyst growth in the absence of forskolin. While more variation within wells was observed within this long-duration assay (attributable to the necessity to refresh compounds and culture media), we observed activity of celastrol at 100 nM, but not 10 nM, when compared to solvent control (Figure 2D).

Celastrol inhibits cyst growth in vivo in iKspCre-Pkd1^{lox,lox} mice and prevents decline of kidney function

To investigate whether the findings *in vitro* could be translated to a response *in vivo*, we tested both celastrol and pyrvinium pamoate in a iKspCre-*Pkd1*^{lox,lox} mouse model, where tamoxifen was used to inactivate the *Pkd1* gene at postnatal day 10 (P10) and P11, to induce rapid cyst formation (Lantinga-van Leeuwen, et al., 2007; Leonhard, et al., 2016). Treatment with pyrvinium pamoate from P13 appeared to be toxic at 1mg/kg/day, and lower dosages did not affect PKD progression in this model (Supplementary Figure S4C and D). We therefore did not further pursue this compound as a possible candidate for PKD treatment. By contrast, celastrol treatment inhibited PKD progression in two separate experiments (Figure 3). The effects of celastrol were first measured at 1 mg/kg/day (7 mice) from P13 to P27, and, even though changes in bodyweight were observed initially, between P13 and P18, celastrol appeared to be well tolerated. In a subsequent independent experiment, we observed similar effects of celastrol at 0.5 mg/kg/day (8 mice) but not at 0.2 mg/kg/day (8 mice) (Supplementary Figure S6A). In line with the *in vitro* findings, celastrol strongly protected kidney function, while lowering cyst burden (Figure 3A-C and Supplementary Figure S6B–E). Renal fibrosis, an important hallmark of ADPKD, is largely driven by activin or TGF-β mediated Smad2/3 activation, resulting in the transcription of target genes including collagens, Plasminogen activator inhibitor-1 and fibronectin-1. We did not find evidence that the Smad2/3 activation underlies cystic expansion in the 3D-cyst model (Supplementary Figure S7B), but we confirmed increased activation in

PKD mice (Supplementary Figure S7A) (Hassane, et al., 2010; Leonhard, et al., 2016). We observed more collagen deposition in PKD kidneys (Figure 3D and E) as well as increased expression of *Pai1*, *Col1a1*, and *Fn1(EDA)* (Supplementary Figure S7A). In celastrol-treated animals at 0.5 and 1.0 mg/kg/day, this expression pattern could partially be restored and PKD-associated fibrosis was lowered (Figure 3D and E). Recently, it has been shown that celastrol reduces renal fibrosis in an Unilateral Ureteral Obstruction model, by enhancing the expression of the anti-fibrotic Cannabinoid Receptor 2 (*Cb2r*) gene (Tang, et al., 2018). We therefore analyzed *Cb2r* expression (Supplementary Figure S7) but show that renal fibrosis in a PKD context increases *Cb2r* expression. The celastrol-treated animals consistently show the opposite expression pattern, which likely reflects the lower cystic load in the celastrol treated animals.

Subtle effects of celastrol on PKD-related signaling

Celastrol has been investigated for other indications where it has shown promising responses, such as inflammatory disorders, cancer and obesity (Kannaiyan, et al., 2011; Liu, et al., 2011, 2015; Venkatesha, et al., 2016). However, the mechanism by which celastrol may affect cyst growth is unclear and we therefore investigated its effects on known PKD-associated signaling (pCREB, pS6, pSTAT3, pERK1/2). Both, in tissue sections and 3D cyst cultures (Figure 4A–C), we found no clear effects of celastrol treatment on the expression pattern of these proteins. Western blotting was used to quantify the expression levels of pS6, pSTAT3, and pERK1/2. Although not statistically significant, we observed a slight reduction of pS6 levels in tissue sections following celastrol exposure; this could indicate an effect of celastrol on mTOR activity (Figure 4B and C).

Since increased proliferation is an important hallmark in ADPKD, we stained kidney sections of PKD mice treated with vehicle or celastrol with the proliferation marker Ki67. Scanned images of these sections were used to set-up an automated nuclear segmentation and $Ki67^+$ nuclei identification method to determine the proliferation indices (Figure 4D and Supplementary methods). The data indicates that there was no visible effect of celastrol on proliferation at the time the mice were sacrificed.

In renal epithelial cells subcellular polarized expression of various ion pumps, including Na^+/K^+-ATPase, control ion gradients and osmotic pressure, which are important for fluid handling. The localization of Na^+/K^+-ATPase in cystic cells has been somewhat controversial

(Terryn, et al., 2011). A shift from basolateral in normal cells to apical in cystic epithelial cells has been reported (Wilson, et al., 2000). However, others reported that the localization in cystic cells remains lateral and to some extent basal but not apical (Brill, et al., 1996). We found mostly basolateral, and cytoplasmic Na^+/K^+-ATPase expression in 3D cultured cysts and in kidneys of PKD mice (Supplementary Figure S8). Fluorescent immunohistochemistry on 3D cultured cysts confirmed lateral and to lesser extent basal expression of Na^+/K^+-ATPase, but no apical expression (Supplementary Figure S9). In renal cysts, the Na^+/K^+-ATPase expression appears to be lower than in healthy tubules, which was confirmed by western blotting (Supplementary Figure S8C). The pattern of Na^+/K^+-ATPase staining was not affected by celastrol treatment, although the expression tends to be reversed to wild type levels, which may be a reflection of the lower cystic load in celastrol treated animals, this reduction was not found to be statistically significant (Supplementary Figure S8C).

Discussion

To discover new drug-like molecules that prevent cystogenesis, we screened a SPECTRUM compound library containing 2320 compounds. Hits were selected and compounds with potentially undesirable characteristics were further eliminated using multiparametric phenotypic profiling of the compound effect. The triterpenoid celastrol and the antihelmintic drug pyrvinium pamoate were selected for further evaluation in an iKspCre-*Pkd1*^{lox,lox} mouse model.

Besides its antihelmintic activity, pyrvinium pamoate is thought to affect WNT/β-catenin and may have potent effects against certain types of cancer (Esumi, et al., 2004; Momtazi-Borojeni, et al., 2018; Polosukhina, et al., 2017; Venerando, et al., 2013; Zhang, et al., 2017). We found that pyrvinium pamoate did not induce beneficial responses in PKD mice, and appeared to cause toxic effects at higher doses. This molecule was therefore not further pursued for treatment of PKD. Since pyrvinium pamoate is used to treat intestinal infections (Smith, et al., 1976), and not designed for i.p. administration, there is a possibility that it cannot reach the kidneys in sufficient concentration to prevent cyst growth while not affecting other tissue types and organs. The toxic effects observed with the dose 1 mg/kg/day in mice were not predicted based on the phenotypic analysis of cultured cysts. While it is possible that this toxicity is related to effects of pyrvinium pamoate on other organs, which may not be captured by cultured renal cysts, it is also possible

that further investigation and fine-tuning of the differential phenotypic effects of toxic substances could help to exclude such substances in the future.

While pyrvinium pamoate did not show a beneficial response in mice, celastrol caused a strong reduction in the growth of renal cysts *in vivo*, while preventing the deterioration of kidney function. A recent study also confirmed the cyst-reducing effects by celastrol in another model for PKD (Chang, et al., 2018). Initially, we observed a reduction in body weight after treatment with celastrol. However, celastrol appeared to be well tolerated and the reduction in body weight could also be related to the reported role of celastrol as a leptin sensitizer (Liu, et al., 2015). While this finding may introduce bias (food restriction is known to ameliorate cystogenesis in patients (Warner, et al., 2016)), we nevertheless consider it unlikely that anti-obesity effects would explain such profound effects *in vivo* and particularly not efficacy *in vitro*.

Phenotypic profiling of 3D cultured cysts and the subsequent evaluation in mice allowed for the identification of celastrol as an inhibitor of cyst growth irrespective of its mechanism of action. To determine through which mechanisms celastrol can affect cyst growth *in vitro* and *in vivo*, we studied the effects on signaling pathways associated with PKD on 3D-cultured cysts and tissue sections. Both in tissue sections and cultured cysts, we observed no effects on pCREB, pSTAT3 and pERK, and, although we observed a small not statistically significant effect of celastrol on pS6 in PKD kidneys, this can also be a reflection of the milder cystic phenotype of the celastrol-treated animals. In addition, Cb2r and Na^+/K^+-ATPase expression studies were not indicative for the mechanism by which celastrol reduces PKD progression. We could confirm a role of TGF-β related signaling in PKD mice, but failed to detect this same involvement in 3D cyst cultures, indicating that this pathway is not causative for cyst growth in this model. Since the 3D cysts are cultured in an already collagen-rich extracellular matrix, this model may not be optimal for studying fibrosis during cystogenesis.

A variety of studies suggested a large number of signaling pathways that may be affected by celastrol including HSP90/Cdc37 (Dal Piaz, et al., 2015; Hieronymus, et al., 2006) and NFκB (Lee, et al., 2006) (for a literature overview see Supplementary Table S2). We therefore consider it likely that celastrol affects cystogenesis by a multi-target mechanism. This idea was further supported by recent research by Zhou et al. (2016), where 66 celastrol-binding proteins were identified, which function in various different processes, including (redox-) metabolism and the ubiquitin proteasome pathway. This multi-target mechanism may be the result of interactions of

celastrol (and other triterpenoids) with thiol groups in many proteins (Liby, et al., 2007; Salminen, et al., 2010; Zhou, et al., 2016). Interestingly, similar Michael acceptor properties have been reported for curcumin (Na and Surh, 2006), a molecule that also delays cystogenesis in mice (Leonhard, et al., 2011). Because these molecules may have different affinity towards different thiol residues, it is possible that they affect other proteins and pathways as a result of concentration changes (Liby, et al., 2007). Celastrol is also known to have antioxidant activity (Wang, et al., 2014), and may therefore reduce kidney damage by induction of cytoprotective genes, as reported for curcumin (Balogun, et al., 2003), which can in turn ameliorate cystogenesis (Happe, et al., 2009; Malas, et al., 2017; Takakura, et al., 2009).

In conclusion, using phenotypic screening, we have identified celastrol as a potent inhibitor of cyst growth. We confirmed the efficacy of celastrol in a juvenile PKD model where it potently protected kidney function and lowered cyst burden. The phenotypic screening approach allowed for the identification of this molecule without knowing its mechanism of action, which is likely not specific for one target. While additional experiments to determine the mechanism of action of celastrol and to establish its safety and efficacy profile are warranted, celastrol may prove to be an interesting treatment option for PKD.

Materials and methods

Additional detailed descriptions of the experimental procedures are included in Supplementary material.

3D cyst culture procedure

Cyst culture and screening were performed as described previously (Booij, et al., 2017). Briefly, cryopreserved mIMCD3 sh*Pkd1* or mIMCD3 *Pkd1*$^{-/-}$ cells were quick-thawed and grown in culture medium (DMEM/F12 Ham's, supplemented with FBS and antibiotics) for 72 hours. Cells were trypsinized and mixed with Cyst-Gel (OcellO) and plated in 384-well plates (Greiner Bio-One). After addition of culture medium, cysts were allowed to form during 72 h (*shPkd1*) or 96 h (*Pkd1*$^{-/-}$) and subsequently exposed to forskolin (Calbiochem) and test compounds for 72 h. Cysts were thereafter fixed and simultaneously stained for F-actin and nuclei for 12–24 h at 4°C. After washing in 1× PBS (Sigma Aldrich) for 24 h, plates were imaged using either a BD

Pathway 855 microscope (BD Bioscience) or ImageXpress Micro XLS (Molecular Devices), with a 4× objective.

Image and data analysis

Image stacks for each well were analyzed and phenotypes were quantified using Ominer software (OcellO) integrated in KNIME Analytics Platform (http://www.knime.org) (Supplementary Figure S1A and C). The 450 phenotypic measurements were *z*-score normalized to plate median or normalized to percent of control. Linear discriminant analysis (LDA) was performed using the 83 least correlating phenotypic parameters (Pearson product-moment correlation coefficient <0.85). LDA was trained on unstimulated (solvent), stimulated (forskolin-treated), and known cytotoxic molecules (daunorubicin, doxorubicin, staurosporin, gambogic acid, epirubicin, at 1 μM) and the trained model was applied to all data. The two resulting linear discriminants were scaled and a small absolute distance (<50) to the unstimulated control group was considered as desirable efficacy.

Compounds

A molecule library containing 2320 compounds (SPECTRUM 2320) was obtained from MicroSource Discovery Systems. Compounds were pre-dissolved to 10 mM in DMSO (Biosolve) and final DMSO content was kept constant at a well-tolerated 0.2% (*v/v*) for all *in vitro* experiments. Celastrol was derived from this library and performed equally well compared to celastrol obtained from another source (Sigma Aldrich).

Animal procedures

The local animal experimental committee of the Leiden University Medical Center (LUMC) and the Commission Biotechnology in Animals of the Dutch Ministry of Agriculture approved all animal experiments performed. Kidney-specific, tamoxifen-inducible Cre-*Pkd1*lox mice (iKspCre-*Pkd1*^{lox,lox}) (Lantinga-van Leeuwen, et al., 2006; Lantinga-van Leeuwen, et al., 2007) received 15 mg/kg Tamoxifen at P10 and P11 to inactivate *Pkd1* to cause rapid cyst formation. Mice received i.p. injections of celastrol, pyrvinium pamoate, or vehicle (5% DMSO + 10% Kolliphor EL in PBS) between P13 and P27. Mice were euthanized at P27 after blood sample collection to measure blood urea levels using Reflotron Technology. Kidneys were halved and

snap frozen or embedded in paraffin. Image scans of Periodic acid-Schiff (PAS)- stained kidney sections were analyzed by an investigator blinded to the treatment. The fibrotic index was calculated as done previously on the basis of Sirius Red staining (Leonhard, et al., 2016).

Immunohistochemistry

Samples were fixated with formaldehyde and embedded in paraffin. Samples were subsequently deparaffinised and subjected to heat-mediated antigen retrieval. Sections were blocked with 0.2% H_2O_2 for 20 min and subsequently pre-incubated for 1 h with 5% normal goat serum in 1% BSA in PBS. Sections were then incubated O/N with anti-pSTAT3 (1:75, Cell Signaling Technology, no. 9145), anti-p-rpS6 (1:100, Cell Signaling Technology, no. 2215), anti-pERK1/2 (1:400, Cell Signaling Technology, no. 4370), anti-Ki67 (1:3000, Nova Castra, NCL Ki67p), anti-pCREB (1:800, Cell Signaling Technology, no. 9198), or anti-Na^+/K^+-ATPase (1:6400, Abcam, ab76020). Immune reactions were revealed using diaminobenzidine and hematoxylin, after incubation of sections with horseradish peroxidase.

Western blotting

NaF, Na2VO4, and protease inhibitor cocktail (Roche) were used to inhibit phosphatase and protease activity. Kidneys were homogenized with RIPA without detergents using Magnalyser technology (Roche) followed by sonication. RIPA with detergents was added and incubated for 45 min at 4°C, after which lysates were centrifuged and supernatants were stored at -80°C. Lysate was subsequently used for SDS-PAGE and immunoblotting. Membranes were blocked for 1 h with 25% sea block blocking buffer (Thermo Fisher Scientific/Pierce) and incubated O/N with anti-pSTAT3 (1:1000), anti-p-rpS6 (1:2000), anti-pERK1/2 (1:1000), anti-Na^+/K^+-ATPase (1:10.000), or anti-α-tubulin (1:2000). DyLight reagents (Perbio Science, no.35571 or no.35518) were used as secondary antibody. Detection and densitometric analysis were carried out using Odyssey Infrared Imaging System (Westburg).

Proliferation index

Kidney sections were stained with anti-Ki67 as described above and scanned for image analysis. Image segmentation and subsequent object extraction was performed using Ominer software (OcellO). Classification of nuclei was achieved by measuring Ki67 staining strength. To

eliminate variation in staining intensity between the outer medulla and cortex, digital background correction was performed. Final Ki67 staining strength was measured as a ratio between blue and red signal.

Statistical analysis

Statistical analyses were performed in Graphpad Prism 7 software using ANOVA with Dunnett's multiple comparison's test unless otherwise stated in figure legends. Results were considered statistically significant for $p<0.05$.

Acknowledgements

The authors would like to thank Lotte Verburg and Kyra Dijkstra for technical assistance.

Funding

T.H.B. and W.N.L. were supported by the Dutch Technology Foundation STW (Project 11823), which is part of The Netherlands Organization for Scientific Research (NWO). G.J.P.v.W. is supported by the Dutch Technology Foundation STW (Project 14410). M.F. was supported by the EU-FP7 — Systems Microscopy NoE (grant no. 258068) and A.J.P. by a grant from the Dutch Kidney Foundation (4OIP12).

Conflict of interest: L.S.P. is co-founder and CSO of OcellO B.V., a drug discovery contract research organization located in Leiden, The Netherlands.

References

Balogun, E., Hoque, M., Gong, P., et al. (2003). Curcumin activates the haem oxygenase-1 gene via regulation of Nrf2 and the antioxidant-responsive element. Biochemical Journal. *371*(Pt 3), 887-895

Booij, T.H., Bange, H., Leonhard, W.N., et al. (2017). High-throughput phenotypic screening of kinase inhibitors to identify drug targets for polycystic kidney disease. SLAS Disc. *22*(8), 974-984

Brill, S.R., Ross, K.E., Davidow, C.J., et al. (1996). Immunolocalization of ion transport proteins in human autosomal dominant polycystic kidney epithelial cells. Proc. Natl. Acad. Sci. USA. *93*(19), 10206-10211

Chang, M.Y., Hsieh, C.Y., Lin, C.Y., et al. (2018). Effect of celastrol on the progression of polycystic kidney disease in a Pkd1-deficient mouse model. Life Sci. *212*70-79

Dal Piaz, F., Terracciano, S., De Tommasi, N., et al. (2015). Hsp90 activity modulation by plant secondary metabolites. Planta Med. *81*(14), 1223-1239

Devuyst, O. and Torres, V.E. (2013). Osmoregulation, vasopressin, and cAMP signaling in autosomal dominant polycystic kidney disease. Curr Opin Nephrol Hypertens. *22*(4), 459-470

Esumi, H., Lu, J., Kurashima, Y., et al. (2004). Antitumor activity of pyrvinium pamoate, 6-(dimethylamino)-2-[2-(2,5-dimethyl-1-phenyl-1H-pyrrol-3-yl)ethenyl]-1-methyl-qu inolinium pamoate salt, showing preferential cytotoxicity during glucose starvation. Cancer Sci. *95*(8), 685-690

Happe, H., Leonhard, W.N., van der Wal, A., et al. (2009). Toxic tubular injury in kidneys from Pkd1-deletion mice accelerates cystogenesis accompanied by dysregulated planar cell polarity and canonical Wnt signaling pathways. Hum. Mol. Genet. *18*(14), 2532-2542

Hassane, S., Leonhard, W.N., van der Wal, A., et al. (2010). Elevated TGFbeta-Smad signalling in experimental Pkd1 models and human patients with polycystic kidney disease. J Pathol. *222*(1), 21-31

Hieronymus, H., Lamb, J., Ross, K.N., et al. (2006). Gene expression signature-based chemical genomic prediction identifies a novel class of HSP90 pathway modulators. Cancer Cell. *10*(4), 321-330

Jung, R.C. (1976). Treatment of intestinal parasitic disease. South. Med. J. *69*(6), 799-804

Kannaiyan, R., Shanmugam, M.K., and Sethi, G. (2011). Molecular targets of celastrol derived from Thunder of God Vine: potential role in the treatment of inflammatory disorders and cancer. Cancer Lett. *303*(1), 9-20

Lantinga-van Leeuwen, I.S., Leonhard, W.N., van de Wal, A., et al. (2006). Transgenic mice expressing tamoxifen-inducible Cre for somatic gene modification in renal epithelial cells. Genesis. *44*(5), 225-232

Lantinga-van Leeuwen, I.S., Leonhard, W.N., van der Wal, A., et al. (2007). Kidney-specific inactivation of the Pkd1 gene induces rapid cyst formation in developing kidneys and a slow onset of disease in adult mice. Hum. Mol. Genet. *16*(24), 3188-3196

Lee, J.H., Koo, T.H., Yoon, H., et al. (2006). Inhibition of NF-κB activation through targeting I kappa B kinase by celastrol, a quinone methide triterpenoid. Biochem Pharmacol. *72*(10), 1311-1321

Leonhard, W.N., Kunnen, S.J., Plugge, A.J., et al. (2016). Inhibition of activin signaling slows progression of polycystic kidney disease. J. Am. Soc. Nephrol. *27*(12), 3589-3599

Leonhard, W.N., van der Wal, A., Novalic, Z., et al. (2011). Curcumin inhibits cystogenesis by simultaneous interference of multiple signaling pathways: in vivo evidence from a Pkd1-deletion model. Am. J. Physiol. Renal. Physiol. *300*(5), F1193-F1202

Leonhard, W.N., Zandbergen, M., Veraar, K., et al. (2015). Scattered Deletion of PKD1 in Kidneys Causes a Cystic Snowball Effect and Recapitulates Polycystic Kidney Disease. J. Am. Soc. Nephrol. *26*(6), 1322-1333

Liby, K.T., Yore, M.M., and Sporn, M.B. (2007). Triterpenoids and rexinoids as multifunctional agents for the prevention and treatment of cancer. Nat. Rev. Cancer. *7*(5), 357-369

Liu, J., Lee, J., Salazar Hernandez, M.A., et al. (2015). Treatment of obesity with celastrol. Cell. *161*(5), 999-1011

Liu, Z., Ma, L., and Zhou, G.B. (2011). The main anticancer bullets of the Chinese medicinal herb, thunder god vine. Molecules. *16*(6), 5283-5297

Malas, T.B., Formica, C., Leonhard, W.N., et al. (2017). Meta-analysis of polycystic kidney disease expression profiles defines strong involvement of injury repair processes. Am. J. Physiol. Renal. Physiol. *312*(4), 806-817

Mangoo-Karim, R., Uchic, M., Lechene, C., et al. (1989). Renal epithelial cyst formation and enlargement in vitro: dependence on cAMP. Proc Natl Acad Sci U S A. *86*(15), 6007-6011

Momtazi-Borojeni, A.A., Abdollahi, E., Ghasemi, F., et al. (2018). The novel role of pyrvinium in cancer therapy. J Cell Physiol. *233*(4), 2871-2881

Na, H.K. and Surh, Y.J. (2006). Transcriptional regulation via cysteine thiol modification: a novel molecular strategy for chemoprevention and cytoprotection. Mol. Carcinog. *45*(6), 368-380

Polosukhina, D., Love, H.D., Moses, H.L., et al. (2017). Pharmacologic Inhibition of beta-Catenin With Pyrvinium Inhibits Murine and Human Models of Wilms Tumor. Oncol. Res. *25*(9), 1653-1664

Salminen, A., Lehtonen, M., Paimela, T., et al. (2010). Celastrol: Molecular targets of thunder god vine. Biochem. Biophys. Res. Commun. *394*(3), 439-442

Smith, T.C., Kinkei, A.W., Gryczko, C.M., et al. (1976). Absorption of pyrvinium pamoate. Clin. Pharmacol. Therapeut. *19*(6), 802-806

Swinney, D.C. (2013). Phenotypic vs. target-based drug discovery for first-in-class medicines. Clin. Pharmacol. Therapeut. *93*(4), 299-301

Takakura, A., Contrino, L., Zhou, X., et al. (2009). Renal injury is a third hit promoting rapid development of adult polycystic kidney disease. Hum. Mol. Genet. *18*(14), 2523-2531

Tang, M., Cao, X., Zhang, K., et al. (2018). Celastrol alleviates renal fibrosis by upregulating cannabinoid receptor 2 expression. Cell Death Dis. *9*(6), 601

Terryn, S., Ho, A., Beauwens, R., et al. (2011). Fluid transport and cystogenesis in autosomal dominant polycystic kidney disease. Biochim. Biophys. Acta. *1812*(10), 1314-1321

Thorne, C.A., Hanson, A.J., Schneider, J., et al. (2010). Small-molecule inhibition of Wnt signaling through activation of casein kinase 1alpha. Nat. Chem. Biol. *6*(11), 829-836

Torres, V.E., Chapman, A.B., Devuyst, O., et al. (2012). Tolvaptan in patients with autosomal dominant polycystic kidney disease. N. Engl. J. Med. *367*(25), 2407-2418

Torres, V.E. and Harris, P.C. (2014). Strategies targeting cAMP signaling in the treatment of polycystic kidney disease. J. Am. Soc. Nephrol. *25*(1), 18-32

Torres, V.E., Harris, P.C., and Pirson, Y. (2007). Autosomal dominant polycystic kidney disease. Lancet. *369*(9569), 1287-1301

Tsai, S.Q., Wyvekens, N., Khayter, C., et al. (2014). Dimeric CRISPR RNA-guided FokI nucleases for highly specific genome editing. Nat. Biotechnol. *32*(6), 569-576

Venerando, A., Girardi, C., Ruzzene, M., et al. (2013). Pyrvinium pamoate does not activate protein kinase CK1, but promotes Akt/PKB down-regulation and GSK3 activation. Biochem. J. *452*(1), 131-137

Venkatesha, S.H., Dudics, S., Astry, B., et al. (2016). Control of autoimmune inflammation by celastrol, a natural triterpenoid. Pathog. Dis. *74*(6), 1-12

Wang, C., Shi, C., Yang, X., et al. (2014). Celastrol suppresses obesity process via increasing antioxidant capacity and improving lipid metabolism. Eur. J. Pharmacol. *744*52-58

Warner, G., Hein, K.Z., Nin, V., et al. (2016). Food restriction ameliorates the development of polycystic kidney disease. J. Am. Soc. Nephrol. *27*(5), 1437-1447

Willey, C.J., Blais, J.D., Hall, A.K., et al. (2017). Prevalence of autosomal dominant polycystic kidney disease in the European Union. Nephrol. Dial. Transplant. *32*(8), 1356-1363

Wilson, P.D., Devuyst, O., Li, X., et al. (2000). Apical plasma membrane mispolarization of NaK-ATPase in polycystic kidney disease epithelia is associated with aberrant expression of the beta2 isoform. Am. J. Pathol. *156*(1), 253-268

Wong, K.F., Yuan, Y., and Luk, J.M. (2012). Tripterygium wilfordii bioactive compounds as anticancer and anti-inflammatory agents. Clin. Exp. Pharmacol. Physiol. *39*(3), 311-320

Zhang, C., Zhang, Z., Zhang, S., et al. (2017). Targeting of Wnt/beta-Catenin by Anthelmintic Drug Pyrvinium Enhances Sensitivity of Ovarian Cancer Cells to Chemotherapy. Med. Sci. Monit. *23*266-275

Zhou, Y., Li, W., Wang, M., et al. (2016). Competitive profiling of celastrol targets in human cervical cancer HeLa cells via quantitative chemical proteomics. Mol. Biosyst. *13*(1), 83-91

Figure Legends

Figure 1 Screening a small-molecule library to identify inhibitors of cyst growth. (**A**) 2320 molecules were ranked according to inhibitory effect on mIMCD3 sh*Pkd1* cyst growth (z-score normalized to plate median). Molecules inhibiting cyst growth relative to forskolin-stimulated control ("Stimulated") included positive control molecules, as indicated by colored circles in the enlarged cut-out. For control molecules, error bars represent standard deviations (SD). For all other molecules, error bars represent ½*difference between two replicate wells. (**B**) Many molecules contained in the library have an antibacterial or antineoplastic mechanism of action. Since for some natural molecules the mechanism of activity is not elucidated, the bioactivity is listed as "unknown". (**C**) The selected 81 cyst growth-inhibiting hits were markedly enriched in antineoplastic, anti-infective, and antihelmintic molecules, compared to **B**.

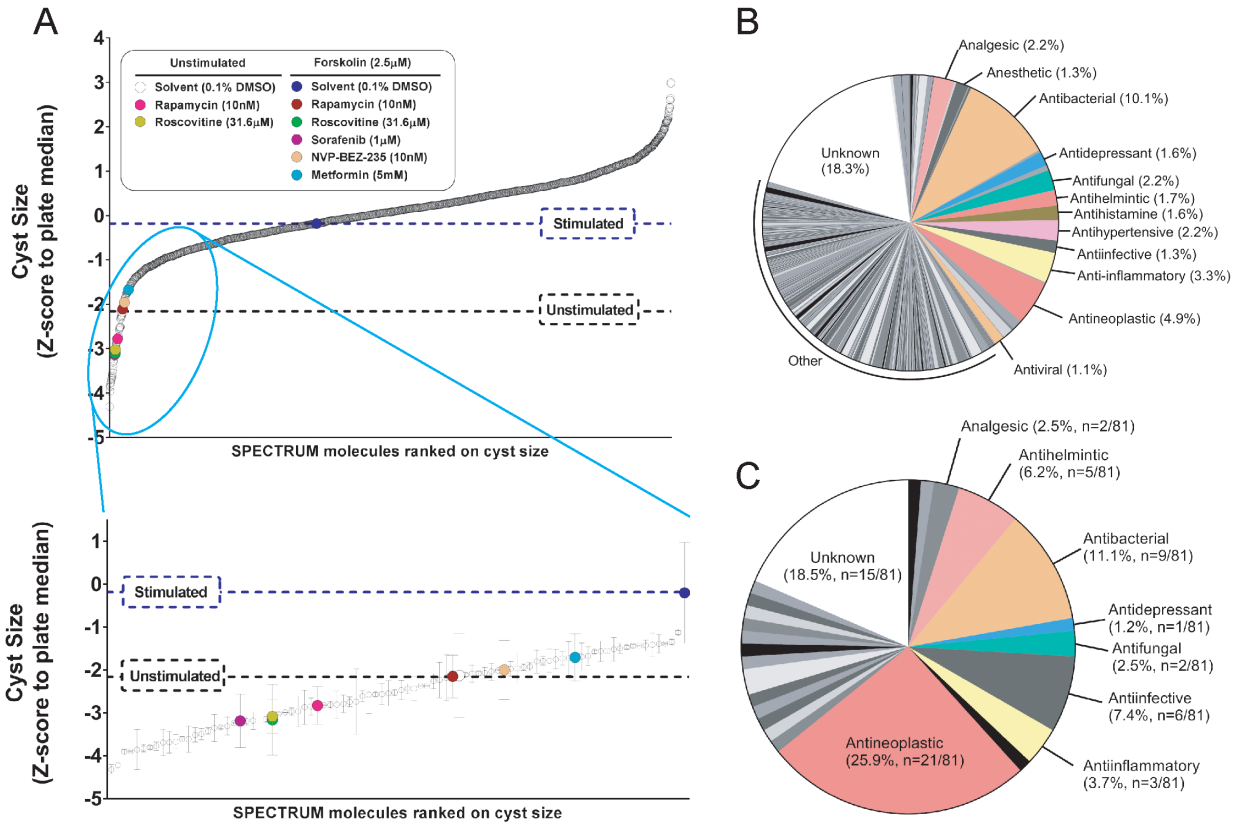

Figure 2 Celastrol inhibits cyst growth dose-dependently. (**A**) Celastrol inhibits mIMCD3 *Pkd1*$^{-/-}$ cyst growth. At the highest concentrations (316 and 1000 nM), cyst size is lower than unstimulated control, possibly corresponding to effects shown in **B** in linear discriminant 2. These experiments were repeated at least three times. (**B**) LDA plot showing efficacy (linear discriminant 1) and toxicity (linear discriminant 2) of celastrol using multiparametric phenotypic measurements on mIMCD3 *Pkd1*$^{-/-}$ cysts. At the left (ringed in blue), the forskolin stimulated large cysts. At the right (ringed in black), the unstimulated small cysts. Larger dot sizes correspond to higher compound concentrations. Celastrol (red dots) is only toxic at the highest concentration. (**C**) Representative images of 3D-cultured mIMCD3 *Pkd1*$^{-/-}$ cysts (cytoskeleton, F-actin) co-exposed with 2.5 μM forskolin and celastrol at different concentrations, or vehicle control (stimulated, 2.5 μM forskolin). The 500×500px cut-out of images taken with the ImageXpress Micro XLS imager are shown for presentation purposes. (**D**) Long-term exposure with celastrol shows inhibition of spontaneous cyst growth over 13 days. The 1000×1000px cut-out of (cytoskeleton, F-actin) images were taken with the BD Pathway 855 imager. Brightness and contrast of all images were enhanced for presentation purposes. Scale bar, 250 μm.

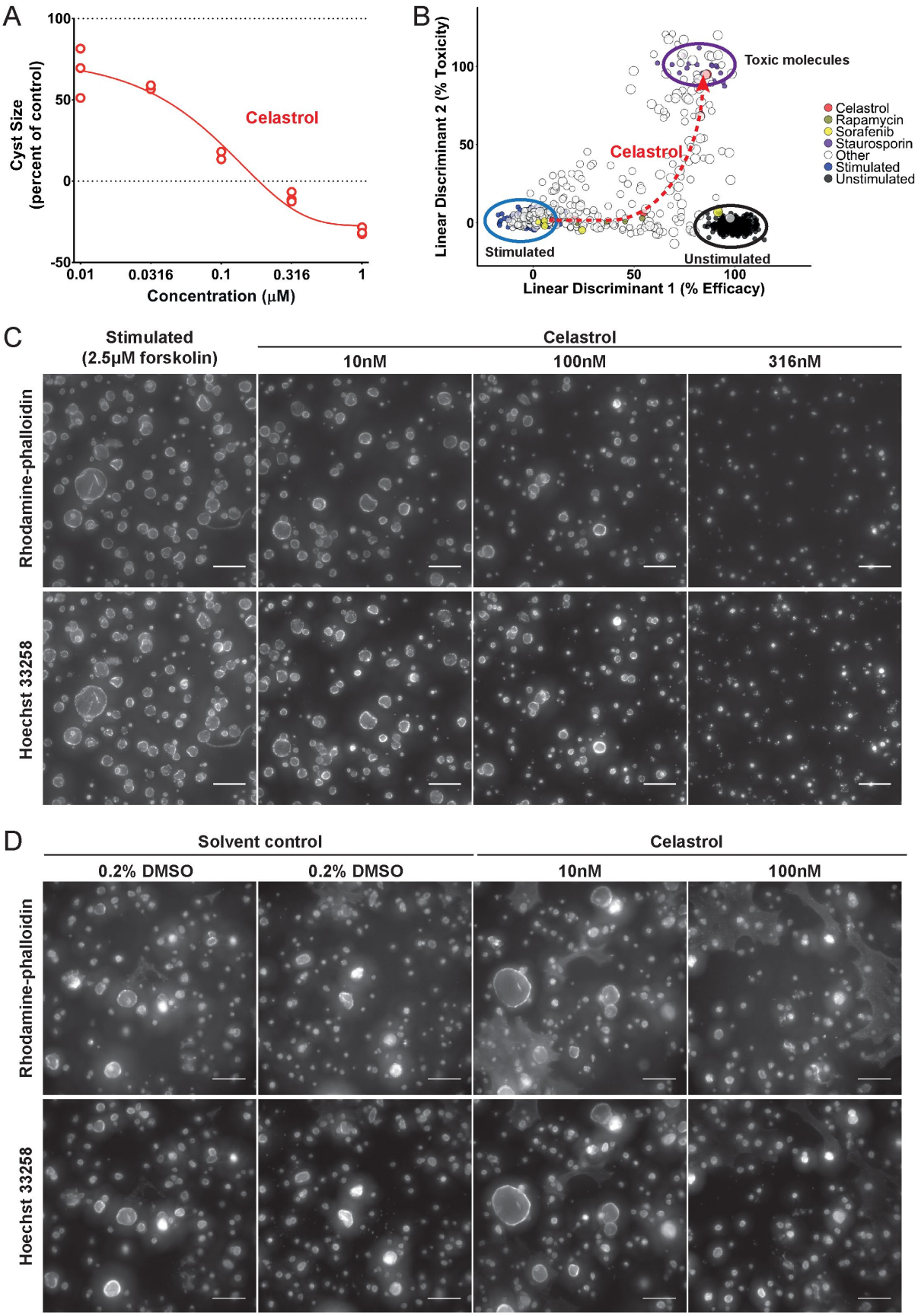

Figure 3 Celastrol inhibits cyst growth *in vivo* in iKspCre-Pkd1^{lox,lox} mice and prevents decline of kidney function. The results presented here combined two independent experiments, where celastrol was first tested at 1 mg/kg/day and later at 0.2 and 0.5mg/kg/day, because the vehicle controls were highly similar. (**A**) Two-kidney weight as percentage of bodyweight of vehicle-treated or celastrol-treated mice at P27. Data shown represent mean±SD and individual data points for all mice. Vehicle-treated (n=16), celastrol 0.2 mg/kg (n=7), 0.5 mg/kg (n=8), and 1.0 mg/kg (n=7). (**B**) Blood urea nitrogen (BUN/Urea) given in mmol/L for vehicle- or celastrol-treated mice as a measurement of kidney function plotted against cystic index, indicating *in vivo* cyst size (disease severity) measured in P27 kidneys after vehicle or celastrol treatment. Vehicle-treated (n=16), celastrol 0.2 mg/kg (n=7), 0.5 mg/kg (n=8), and 1.0 mg/kg (n=7). (**C**) Representative images of renal histology of P27 kidneys showing that renal cysts were reduced after celastrol treatment for 0.5 and 1.0 mg/kg treatment groups, compared to vehicle. Additional tissue sections are presented in Supplementary Figure S6 to illustrate experimental variation. (**D**) Fibrotic index as measured by intensity of Sirius Red signal (normalized to vehicle control) for vehicle-treated (n=16), 0.2 mg/kg/day celastrol-treated (n=7), 0.5 mg/kg/day celastrol-treated (n=7), and 1.0 mg/kg/day celastrol-treated (n=7) mice. (**E**) Representative Sirius Red-stained sections of celastrol-treated (0.2, 0.5, and 1.0 mg/kg/day) P27 kidneys, compared to vehicle control. Statistical significance was assessed with ordinary one-way ANOVA with Dunnett's multiple comparisons test. *$p<0.05$, **$p<0.01$, ***$p<0.001$.

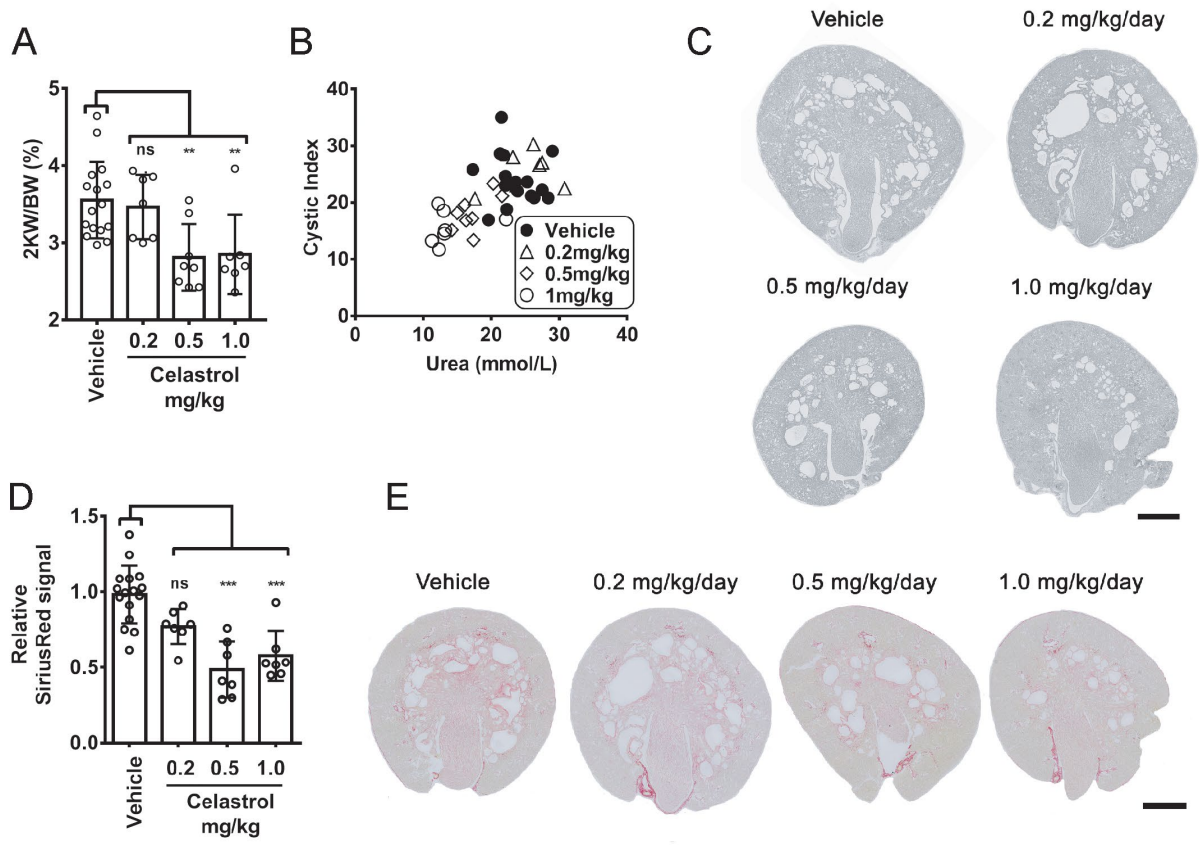

Figure 4 Subtle effects of celastrol on PKD-related signaling. (**A**) Representative images of sections of 3D-cultured mIMCD3 *Pkd1*$^{-/-}$ cysts, treated with solvent (DMSO), celastrol, or rapamycin and stained for pS6 (mTOR activity), pCREB, pSTAT3, and pERK1/2. Scale bar, 100 µm. (**B**) Tissue sections after staining for pS6, pCREB, pSTAT3, and pERK1/2 of vehicle-treated and celastrol-treated mice (1 mg/kg/day). To be able to judge the expression pattern of the proteins, images were made in areas that were either minimally cystic in vehicle-treated mice or cystic in vehicle- or celastrol-treated mice (scale bar, 50 µm). The expression pattern of the minimally cystic regions is comparable to the pattern in WT tissue sections (data not shown and (Leonhard, et al., 2011; Leonhard, et al., 2015)) where cystic and non-cystic tissue was present. (**C**) Western blotting and densitometric quantification of combined blots for pS6, pSTAT3, pERK1/2, and tubulin of vehicle-treated and celastrol-treated mice (1 mg/kg/day). Potential differences between WT controls versus PKD vehicle and PKD vehicle versus PKD celastrol

were tested using Student's t-test: *p<0.05, 'ns' indicates not statistically significant. (**D**) Ki67 quantification. Upper panel shows processed inverted images of a Ki67-stained kidney section (yellow signal is Ki67 negative, blue signal is Ki67 positive) masking either the cortex (upper middle) or outer medulla (OM, upper right). Lower panel shows the raw signal of a section with Ki67 staining, including a magnification of the raw signal and processed signal showing the nuclear segmentation and Ki67-positive (blue) or Ki67-negative (yellow) nuclei. The quantification of the proliferation index (% of Ki67-positive nuclei) is shown at the right: vehicle (n=19 mice), 0.2 mg/kg celastrol (n=7 mice), 0.5 mg/kg (n=8 mice), 1.0 mg/kg (n=11 mice).